Supplement of Atmos. Chem. Phys., 20, 829–863, 2020
https://doi.org/10.5194/acp-20-829-2020-supplement

Atmospheric Chemistry and Physics
Open Access
EGU

Supplement of

Dust Constraints from joint Observational-Modelling-experiMental analysis (DustCOMM): comparison with measurements and model simulations

Adeyemi A. Adebiyi et al.

Correspondence to: Adeyemi A. Adebiyi (aadebiyi@ucla.edu)

1. Supplementary Figures

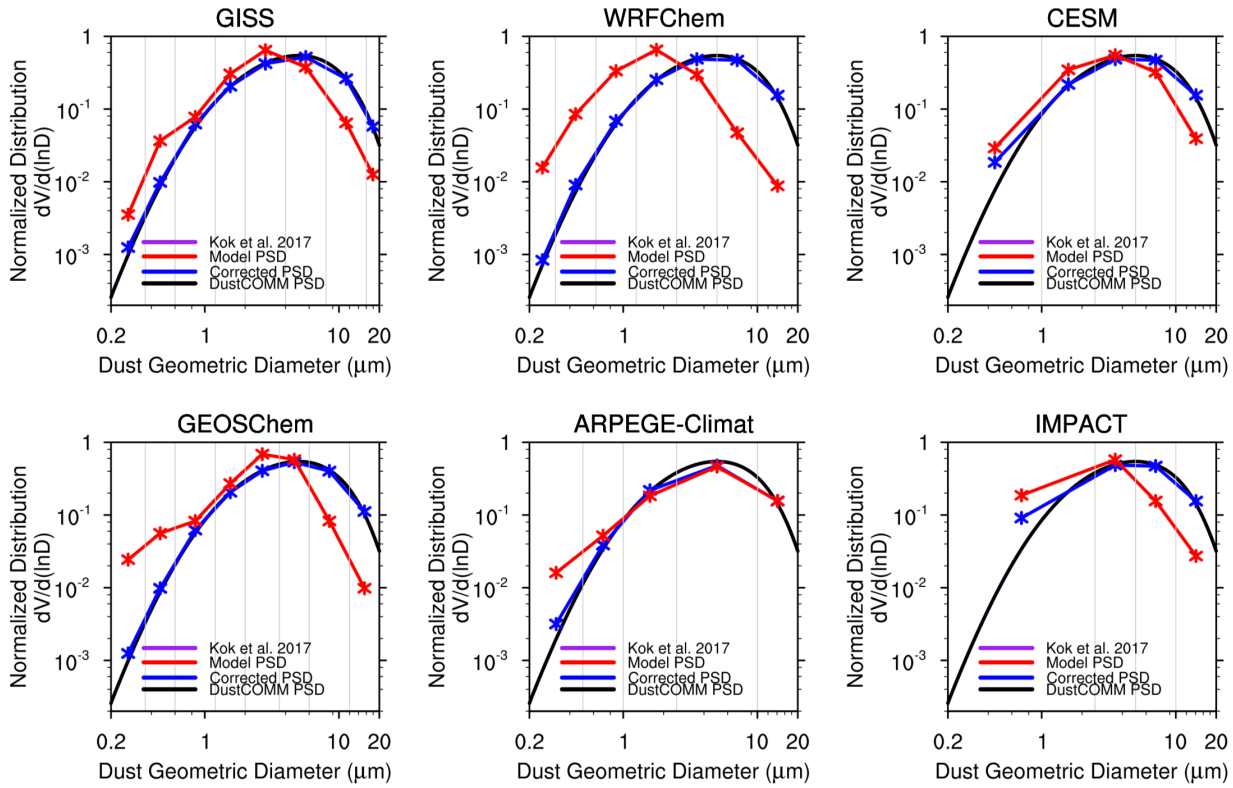

Figure S-1: The globally-averaged size distributions for each model normalized between 0.2 and 20 µm. It shows the model uncorrected dust size distribution (red lines), corrected dust size distribution (blue lines), Kok et al. 2017, and the final constrained DustCOMM dust size distribution with the sub-bins (black lines). Note that since the constrained DustCOMM dust size distribution forced to that of Kok et al., 2017, the lines overlap.

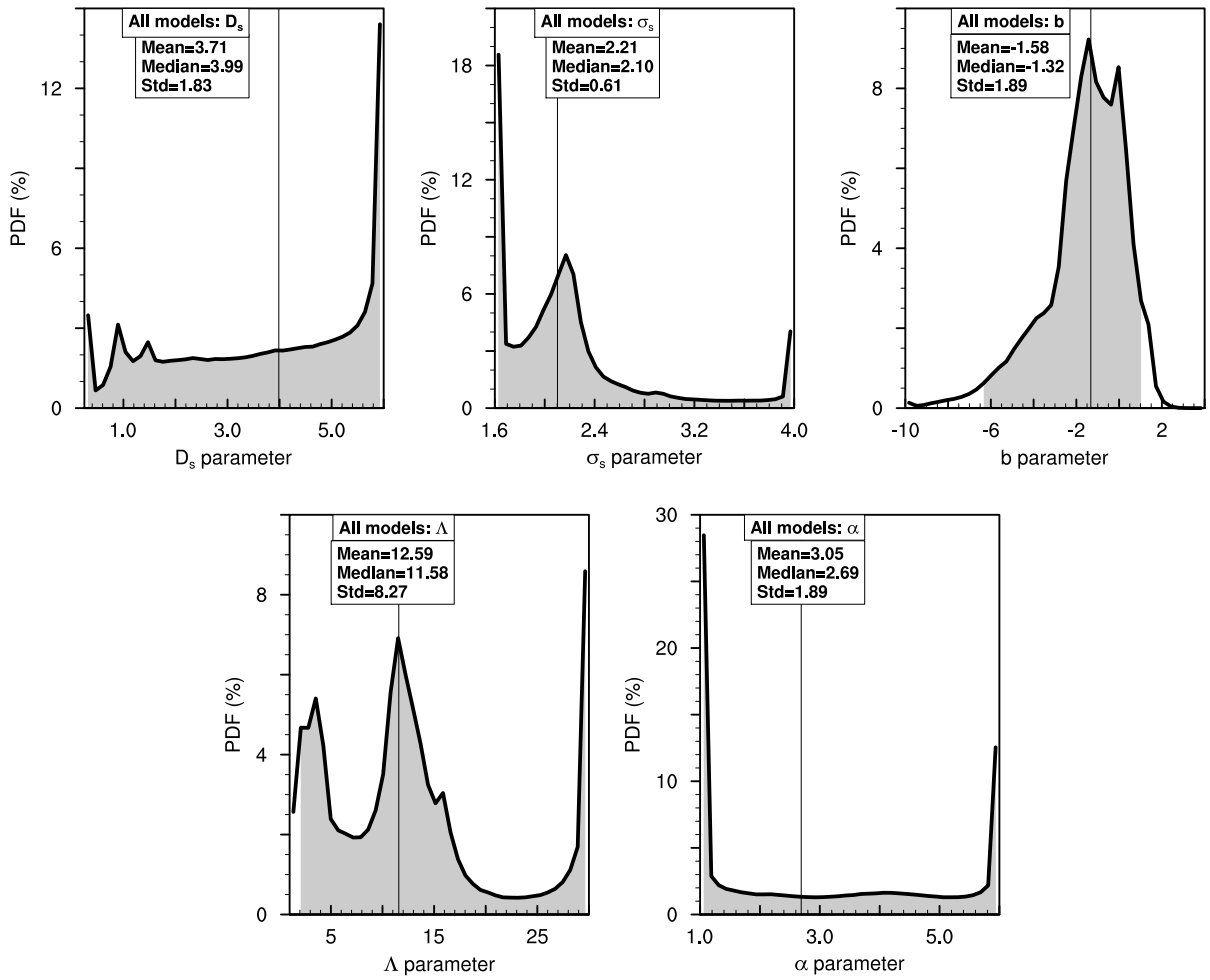

Figure S- 2: Probability distribution of the parameters for the generalized analytical function describing the atmospheric dust size distribution. See section 2.1.2 for details. The shaded regions denote the 95% confidence intervals of each distribution.

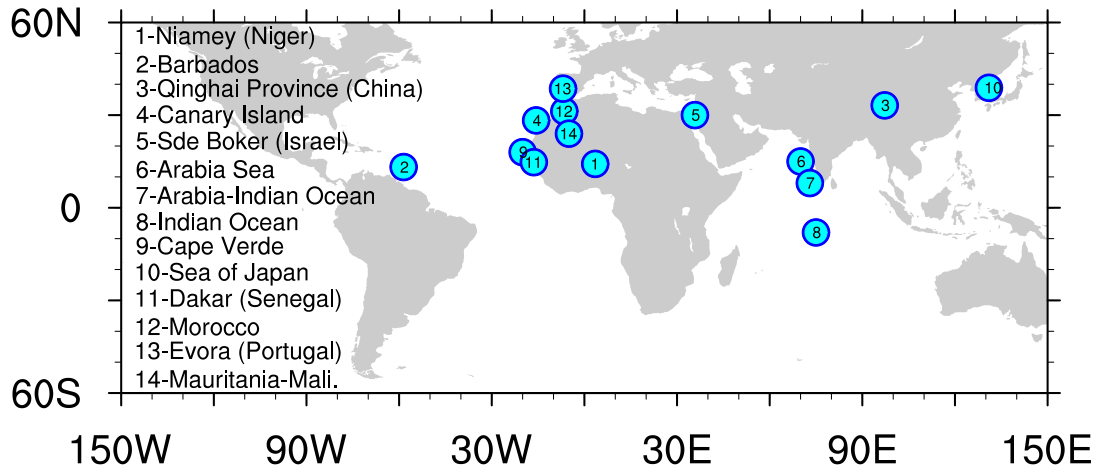

Figure S- 3: Map showing the locations of measurements for evaluation used in this study (Table 2). The measurements in Table 2 that corresponds to the numbers are as follows:
#1 – D'Almeida & Schutz, (1983), Osborne et al., 2008, Chou et al., 2008;
#2 – Li et al., 1996, Jung et al., 2013, Weinzierl et al., 2017;
#3 – Li et al., 2000;
#4 – Maring et al., 2000, Otto et al., 2007; Ryder et al., 2013a
#5 – Andreae et al., 2002;
#6 – Quinn et al., 2002;
#7 – Quinn et al., 2002;
#8 – Quinn et al., 2002;
#9 – Haywood et al., 2003, Kandler et al., 2011, Weinzierl et al., 2017, Ryder et al., 2018;
#10 – Clarke et al. 2004;
#11 – McConnell et al., 2008;
#12 – Weinzierl et al., 2009, Kandler et al., 2009;
#13 – Wagner et al., 2009;
#14 – Ryder et al., 2013b

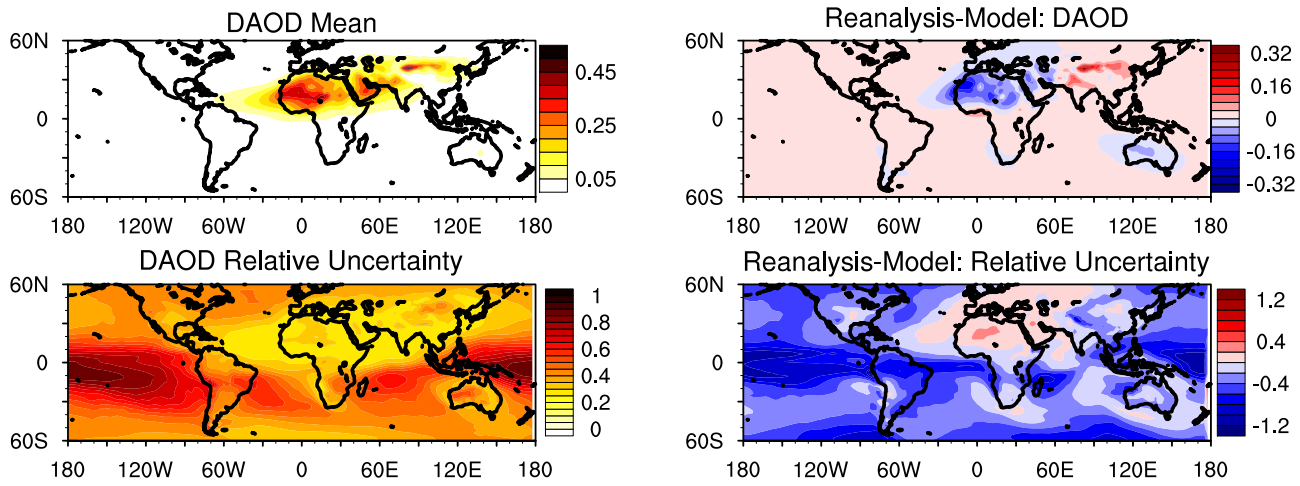

Figure S- 4: Annually-averaged ensemble mean and relative uncertainty of reanalysis dust aerosol optical depth (left panel). See section 3.2 for details Right panel shows the difference between the reanalysis dataset and the model ensemble dust aerosol optical depth.

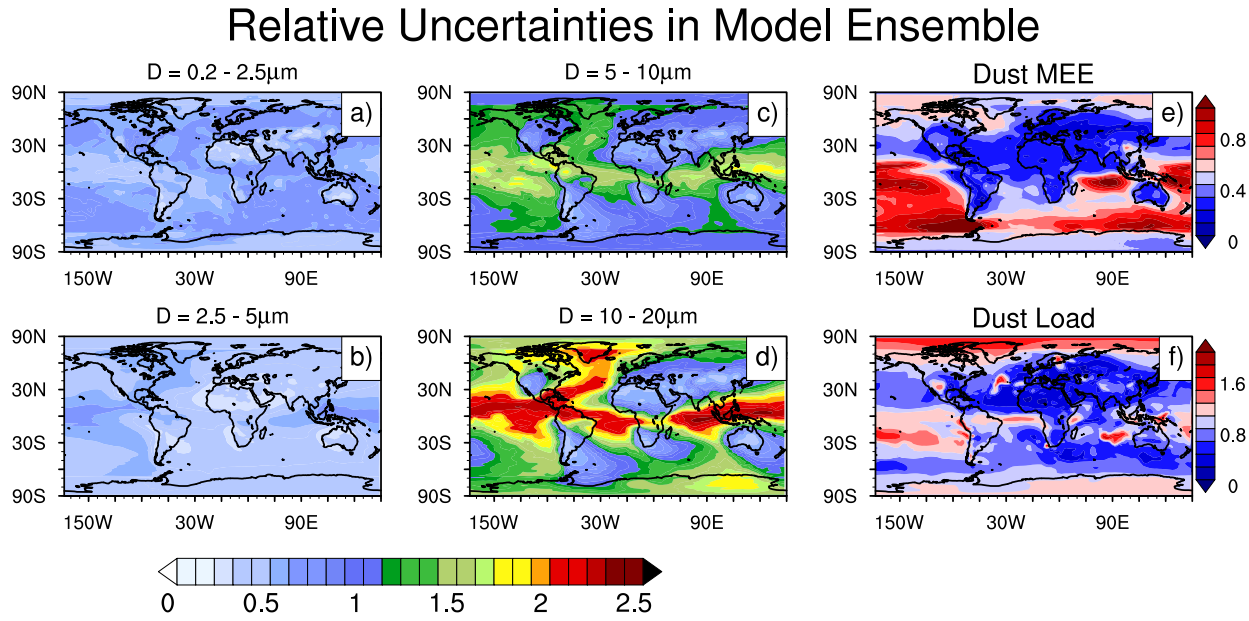

Figure S- 5: Spatial distributions of model ensemble relative uncertainties for (a-d) the dust mass fraction in the diameter range between $0.2-2.5\mu m$, $2.5-5\mu m$, $5-10\mu m$, *and* $10-20\mu m$; *(e) the dust mass extinction efficiency (MEE), and (f) dust load.*

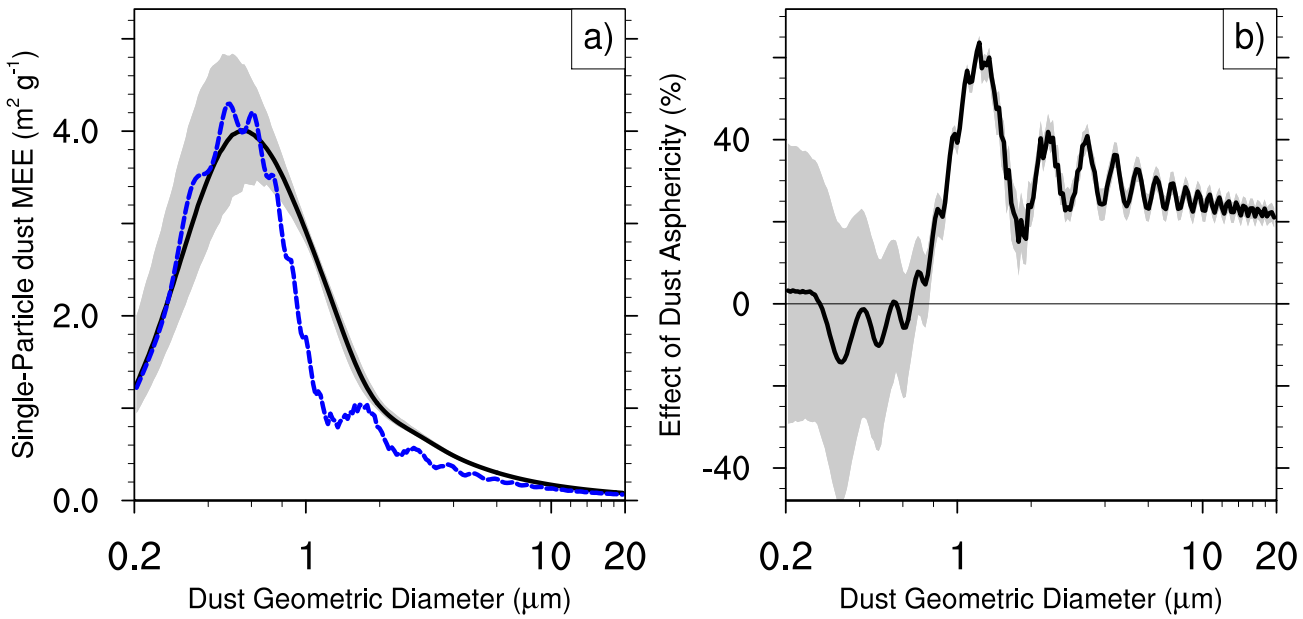

Figure S- 6: (a) Globally-averaged Single-particle DustCOMM dust mass extinction efficiency (MEE; Black line) and one calculated from Mie theory (blue line); (b) the effect of dust asphericity shown as the percentage differences between the dust MEE from DustCOMM and the one from Mie theory. All the black lines present the median of the distribution for each diameter, while the grey shade is the 95% confidence interval. The DustCOMM dust MEE leverages observational constraints on dust shape and dust size distribution (see section 2 in text). In contrast, the blue dashed line denotes the dust MEE calculated from Mie theory, which uses the assumption that dust particles are spherical.

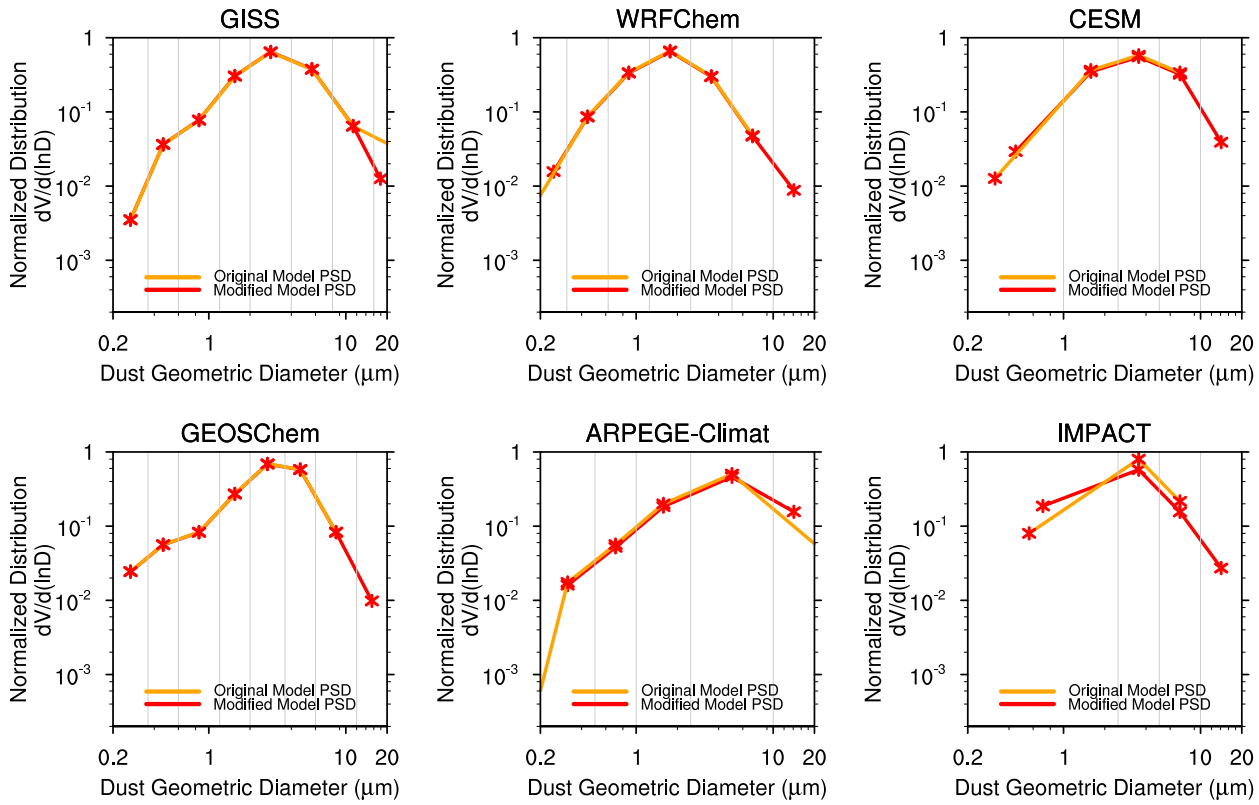

Figure S-7: The original and modified globally-averaged dust size disttribution for each model simulation.

2. Global model simulations

We describe here the model simulations used in this study. The GISS, CESM and GEOS-Chem models are described in detail in Kok et al. (2017) and the references therein (see section 5 of their supplementary document), while the simulations with the WRF-Chem, ARPEGE-Climat and IMPACT models are described below.

2.1.1 WRF-Chem

We use the version of WRF-Chem model (Grell et al., 2005) that is improved by the University of Science and Technology of China (Zhao et al., 2013). This version uses the quasi-global channel configuration with the periodic boundary conditions in the zonal direction and 360 × 145 grid cells (180° W-180° E, 67.5° S-77.5° N) to perform the simulations at 1° horizontal resolution, 35 vertical layers up to 50 hPa, and for the period of 2007-2016. The meteorological initial and lateral meridional boundary conditions are derived from the National Center for Environmental Prediction final analysis (NCEP/FNL) data. In addition, the model simulated winds and atmospheric temperature are nudged towards the NCEP/FNL reanalysis data with a nudging timescale of 6 hr (Stauffer & Seaman, 1990). Furthermore, the simulation uses MOSAIC (Model for Simulation Aerosol Interactions and Chemistry) aerosol module (Zaveri et al., 2008) coupled with the CBM-Z (carbon bond mechanism) photochemical mechanism (Zaveri and Peters, 1999). This aerosol model uses the bin approach with eight discrete size bins to represent aerosol size distributions (Fast et al., 2006). All major aerosol compositions are simulated in the model, including the sulfate, nitrate, ammonium, black carbon, organic matter, sea-salt, and mineral dust. The MOSAIC aerosol scheme also includes physical and chemical processes of nucleation, condensation, coagulation, aqueous phase chemistry, and water uptake by aerosols. More details, including the model physics scheme used, can be found in Zhao et al. (2013).

Vertical dust emission fluxes are calculated as described in Zhao et al. (2010) based on the GOCART dust emission scheme (Ginoux et al., 2001). The emitted dust particles are distributed into the MOSAIC aerosol size bins following a theoretical expression that is based on the physics

of scale-invariant fragmentation of brittle materials derived by Kok (2011). For MOSAIC 8-bin, dust particles are emitted into eight size bins with mass fractions of 10^{-6} %, 10^{-4} %, 0.02%, 0.2%, 1.5%, 6%, 26%, and 45%, respectively. The dry deposition of aerosol mass and number is simulated following the approach of Binkowski & Shankar (1995), which includes both turbulent diffusion and gravitational settling. Wet removal of aerosols by grid-resolved stratiform clouds and precipitation includes in-cloud removal (rainout) and below-cloud removal (washout) by impaction and interception, following Easter et al. (2004) & Chapman et al. (2009). Cloud-ice-borne aerosols are not explicitly treated in the model, but the removal of aerosols by the droplet freezing process is considered. Convective transport and wet removal of aerosols by cumulus clouds follow Zhao et al. (2010, 2013).

The AOD is computed as a function of wavelength for each model grid box. Aerosols are assumed internally mixed in each bin (i.e., a complex refractive index is calculated by volume averaging for each bin for each chemical constituent of aerosols). The Optical Properties of Aerosols and Clouds (OPAC) data set (Hess et al., 1998) is used for the shortwave and longwave refractive indices of aerosols, except that a constant value of 1.53+0.003i is used for the SW refractive index of dust following Zhao et al. (2010, 2011). A detailed description of the computation of aerosol optical properties in WRF-Chem can be found in Fast et al. (2006) & Barnard et al. (2010).

2.1.2 IMPACT

The global chemical transport model used in this study is a coupled gas-phase (Ito et al., 2007) and aerosol chemistry version (Liu et al., 2005) of the Integrated Massively Parallel Atmospheric Chemical Transport (IMPACT) model (Rotman et al., 2004). A detailed description can be found in Ito & Kok (2017) and references therein. The IMPACT model is driven by assimilated meteorological fields from the Goddard Earth Observation System (GEOS) of the NASA Global Modeling and Assimilation Office (GMAO) with a horizontal resolution of 2.0° × 2.5° and 59 vertical layers up to 0.01 hPa. The model simulates the emissions, chemistry, transport, and deposition of major aerosol species (Liu et al., 2005) and their precursor gases (Ito et al., 2007). IMPACT takes into account emissions of primary aerosols and precursor gases of secondary aerosols such as sulfate, nitrate, ammonium and oxalate. Mineral dust aerosols are distributed

among 4 bins in the model. A total dust source is dynamically calculated by a physically-based dust emission scheme (Kok et al., 2014a, 2014b) in conjunction with satellite products of vegetation cover and soil moisture in the model (Ito & Kok, 2017). The chemical composition of mineral dust aerosols may change dynamically from that in the originally emitted aerosols due to reactions with gaseous species.

Dry deposition of aerosol particles uses a resistance-in-series parameterization (Zhang et al., 2001). Gravitational settling is also taken into account (Rotman et al., 2004; Seinfeld & Pandis, 2016). Aerosols and soluble gases can be incorporated into cloud drops and ice crystals within cloud (rainout), collected by falling rain and snow (washout), and be entrained into wet convective updrafts (Liu et al., 2001; Rotman et al., 2004; Ito et al., 2007; Ito & Kok, 2017). The aging of dust and combustion aerosols from hydrophobic to hydrophilic enhances their dry and wet deposition. Hygroscopic growth of mineral dust and combustion aerosols in gravitational settling uses the Gerber (1991) scheme, including the particle growth due to sulfate, ammonium, and nitrate associated with the particles (Liu et al., 2005; Xu & Penner, 2012). Scavenging efficiencies for mineral dust and combustion aerosols in wet deposition are calculated based on the amount of sulfate, ammonium and nitrate coated on the particles (Liu et al., 2005; Xu & Penner, 2012).

The AOD at 550 nm is calculated online using a look-up table as a function of wavelength and size parameter, following Xu & Penner (2012). Five types of aerosols (i.e., carbonaceous aerosols from anthropogenic combustion, carbonaceous aerosols from open biomass burning, dust, sulfate, and sea salt) were assumed to be externally mixed in each size bin, while sulfate, ammonium, and nitrate coated on each aerosol was internally mixed within each aerosol type and size bin. The refractive index for internally mixed aerosols is calculated based on the volume weighted mixture for each aerosol type and size bin.

2.1.3 ARPEGE-Climat

This study uses the global climate model from CNRM, namely ARPEGE-Climat, in its version 6 used in the CMIP6 exercise, with a horizontal resolution of ~1.4° and 91 vertical levels (Michou et al., 2015). ARPEGE-Climat includes an interactive tropospheric aerosol scheme, named

TACTIC (Tropospheric Aerosols for ClimaTe In CNRM), able to represent the main anthropogenic and natural aerosol types in the troposphere. Originally developed in the GEMS/MACC project (Morcrette et al., 2009), this scheme has been adapted to the ARPEGE/ALADIN-climate code (Michou et al., 2015; Nabat et al., 2015). Aerosols are included through sectional bins, separating desert dust (6 size bins whose limits are 0.1, 0.2, 0.5, 1.0, 2.5, 10.0 and 100 μm), sea-salt (3 bins whose limits are 0.03, 0.5, 5.0 and 20.0 μm), sulfate (1 bin, as well as 1 additional variable for sulfate precursors considered as SO2), organic matter (2 bins: hydrophobic and hydrophilic particles) and black carbon (2 bins: hydrophobic and hydrophilic particles) particles. All these 15 species are prognostic variables in the model, submitted to transport (semi-lagrangian advection, and convective transport), dry deposition, in-cloud and below-cloud scavenging. The interaction with shortwave and longwave radiation, is also taken into account through optical properties (extinction coefficient, single scattering albedo and asymmetry parameter) calculated using the Mie theory. Sulfate, organic matter and sea salt concentrations are used to determine the cloud droplet number concentration following Menon et al. (2002), thus representing the cloud-albedo effect (1st indirect aerosol effect).

Focusing more on dust aerosols, emissions are fully interactive, based on the parameterization of Marticorena & Bergametti (1995) which provides the saltation flux depending on surface wind and soil characteristics. The latter consist in the roughness length and the sand/clay/silt fractions, which are based on the ECOCLIMAP database (Masson et al., 2003). The distribution of the resulting emitted dust vertical flux follows then the study of Kok (2011), assuming an analogy with the fragmentation of brittle materials. The six dust size bins have the following effective diameters: 0.09, 0.18, 0.4, 0.9, 3.7 and 13.2 μm. Dry deposition (for the 6 dust bins) and sedimentation (only applied to the two coarsest size bins) are calculated from fixed vertical speeds (respectively Wisely and Hicks, 2000, and Thompson, 2005). Wet deposition includes below-cloud and in-cloud scavenging. The latter relies on the parameterization of Giorgi & Chameides (1986), assuming a fraction of dust aerosols included in droplets equal to 0.1 for the two finest bins and 0.2 for the 4 other bins.

In the present study, a five-year simulation (2004-2008) has been carried out using the ARPEGE-Climat model and its interactive aerosol scheme.

3. Description of the reanalysis datasets

3.1. MERRA-2 Aerosol Reanalysis

The MERRA-2 is the second version of the MERRA atmospheric reanalysis product from the NASA Global Modeling and Assimilation Office (Gelaro et al., 2017), with updates on the reanalysis system to include addition of more observational platforms and correction of known limitations from previous MERRA version (Mccarty et al., 2016), as well as improvement to the Goddard Earth Observing System -5 (GEOS-5) atmospheric general circulation model, used as the base model for the global assimilation system (Mccarty et al., 2016). For the first time, meteorological and aerosol observations (which include bias-corrected aerosol optical depth from MODIS, AVHRR, MISR – over desserts, and ground-based AERONET instruments) are jointly assimilated into MERRA-2, with the aerosol fields simulated with radiatively-coupled version of Goddard Chemistry, Aerosol, Radiation and Transport model (GOCART) (Colarco et al., 2010). GOCART treats aerosol particles as externally mixed, with dust particles provided in five non-interacting bins (Randles et al., 2017). The dust emission in GOCART is based on Ginoux et al. (2001), which depend on wind speed, following the parameterization of Marticorena & Bergametti (1995). Aerosol loss processes include dry deposition, large-scale wet removal, and convective scavenging. While the dry deposition is mostly model dependent, the precipitation-induced aerosol deposition however, depends largely on the assimilated global precipitation information in MERRA-2 (Reichle et al., 2014, 2017). MERRA-2 aerosol properties are available from 1980 onward, but the number of observations assimilated is more than doubled after the year 2003 (Fig. 3 in Randles et al., 2017). MERRA-2 is available for 3-hourly temporal resolution, and 1.5^{o} X 1.5^{o} horizontal fixed spatial resolution.

We use the monthly averages (calculated from daily means) of MERRA-2 DAOD to construct the seasonal and climatological DAOD values between 2003 and 2012. Aerosol products from MERRA-2 have been validated against independent observation (Buchard et al., 2017; Randles et al., 2017), especially for the aerosol optical depth. It is worth noting here also that only AOD is directly constrained by the assimilation in MERRA-2, while other non-analyzed, non-constrained

aerosol properties, like the vertical distribution and aerosol speciation are mostly model-dependent, thereby providing a possible source of uncertainty in the MERRA-2 DOAD reanalysis.

3.2. NAAPS

The Navy Aerosol Analysis and Prediction System (NAAPS) is an offline aerosol transport model (Lynch et al., 2016) driven by the Navy Operational Global Analysis and Prediction System (NOGAPS; Hogan & Rosmond, 1991; Hogan & Brody, 1993). The quality-assured and quality-controlled MODIS and MISR aerosol optical depth are assimilated through the Navy Atmospheric Variational Data Assimilation System (NAVDAS; Zhang et al., 2008), that became operational in 2010. Details on the aerosol model dynamics, emission and sink processes can be found in Lynch et al. (2016). NAAPS contains dust, sea salt, smoke, SO2, and other anthropogenic and biogenic fine particles, all of which are treated as externally mixed. The dust emission in NAAPS is based on Ginoux et al. (2001) erodibility map, with regional source tuning constrained by space-based and ground-based AOT observations (Lynch et al., 2016). While dust removal processes include dry deposition and wet removal, the dry deposition over ocean is adjusted based on assimilated AOT, and the wet deposition is constrained by satellite-based precipitation information retrieved from NOAA Climate Prediction Center MORPHing technique data (CMORPH; Joyce et al., 2004). NAAPS aerosol optical depth are available at 6 h temporal resolution, and 1^{o} X 1^{o} spatial resolution. For consistency with other reanalysis data, seasonal and climatological averages of AOT is also calculated for 2003 to 2012, using monthly averages. Reanalyzed NAAPS coarse and fine-mode AOT have good agreement with ground-based AOT from AERONET stations (Lynch et al., 2016). Similar to MERRA-2 reanalysis, NAAPS does not assimilate aerosol vertical information or speciation, hence the relative dust vertical profiles are uniformly varied, along with other aerosol species, to match the posterior AOT.

3.3. JRAero

The Japanese Reanalysis for Aerosol (JRAero) version 1.0 is produced by the Meteorological Research Institute (MRI) of the Japan Meteorological Agency. The global reanalysis product uses a global aerosol transport model named MASINGAR mk-2 (Model of Aerosol Species IN the

Global AtmospheRe; Yukimoto et al., 2012), which consist an updated dust emission scheme (Yumimoto et al., 2017), when compared to the previous version of MASINGAR (Tanaka et al., 2003). MASINGAR mk-2 is coupled to an atmospheric general circulation model, also developed at MRI (Yoshimura and Yukimoto, 2008; Yukimoto et al., 2012), while the aerosol assimilation is done every 6 hours using a two-dimensional variational method (MASINGAR/2D-Var, similar to NAAPS-NAVDAS). Only the level 3 bias-corrected MODIS AOD, developed by the US Naval Research Laboratory (NRL) and the University of North Dakota (Zhang & Reid, 2006 Hyer, et al., 2011; Shi et al., 2011), is assimilated into MASINGAR mk-2, and this data is largely unavailable over the deserts due to the stringent quality-control procedure (e.g. Yumimoto et al., 2017). Aerosol particles in the model are treated as externally mixed, with mineral dust carried in ten discrete particle bins (Yumimoto et al., 2017). The updated dust emission uses the wind erosion model developed by Shao et al. (1996), with erodibility factors for vegetation cover, snow cover, land-use type, and soil type (Tanaka and Chiba, 2005). Unlike MERRA-2 and NAAPS, both aerosol dry deposition and wet removal processes in MASINGAR mk-2 are model-dependent. Dry deposition in the model depends on the dry deposition velocity, which employs the resistance analog model (Seinfeld and Pandis, 2006), while the wet deposition process follows the parameterization of Giorgi & Chameides (1986) for in-cloud scavenging, and the procedure detailed in Tanaka & Chiba (2005) for below-cloud scavenging. JRAero is available for the period between 2011 and 2015, at 6 hours temporal resolution, and approximately 1.1^{o}x1.1^{o} spatial resolution. We use the monthly averages of JRAero DAOD between 2011—2015 to construct the seasonal and climatological global DAOD values. Though the averaging period of 2011—2015, is different from other reanalysis product used, the spatial distribution of DAOD is largely consistent with other reanalysis products, albeit slightly smaller magnitude.

3.4. CAMSiRA

The Copernicus Atmosphere Monitoring Service (CAMS) interim Reanalysis (CAMSiRA) is a global reanalysis of atmospheric composition (Flemming et al., 2017). It uses a modified version of the European Centre for Medium-Range Weather Forecasts (ECMWF) Integrating Forecasting System for Composition (C-IFS) (Flemming et al., 2015). The aerosol model is based on the LMDZ model of Laboratoire de Météorologie Dynamique aerosol model (Reddy et al., 2005) that

uses a bulk–bin scheme simulating desert dust, sea salt, organic carbon, black carbon, and sulfate aerosols (Morcrette et al., 2009). The wet and dry deposition are also modelled with different parameterizations. The wet deposition is based on Jacob et al. (2000) which account for sub-grid scale clouds and precipitation. Dry deposition is based on pre-calculated monthly mean deposition velocities following Wesley (1989). The C-IFS uses a four-dimensional variational (4D-VAR) data assimilation technique to combine satellite observations with chemistry-aerosol modelling. Aerosol optical depth is assimilated mainly from MODIS, with the variational bias correction scheme developed at ECMWF (Inness et al., 2015). The mass mixing ratios of O3 and CO are also assimilated from various instruments as additional control variables. CAMSiRA is available for the period between 2011 and 2017, at 3 hours temporal resolution, and approximately 1.1^{o}x1.1^{o} spatial resolution. We use the monthly averages of CAMSiRA DAOD to construct the seasonal and climatological global DAOD values.

4. Summary of measurements collected from literature and used for evaluation

4.1. D'Almeida (1987) – Ground Station – PSD only

Aerosol particles are collected on microsorban-98 fiber filter, with size 20cm by 25 cm described in D'Almeida and Schutz (1983). This filter has a low flow resistance, and a high particle retention capacity. The filter is then dissolved in an organic liquid, such as xylene, to convert the dust particles into liquid suspensions. The resulting suspension is counted with scanning electron microscope (See the Fig. 1 in D'Almeida and Schutz (1983)). The procedure avoids charging effects on the sample surface, to guarantee unbiased magnification of the samples up to 30,000 times. The analysis was further corrected for collection efficiency of the filter. We use the average measurements that were taken over three sites between February-March 1979, and January-February 1982. These locations are: Matam (northeast Senegal) Timbuktu (Mali), and Agadez (Niger) and shown in Fig. 3 of D'Almeida (1987). Dust particles were measured for sizes larger than 100μm, but we use size distribution up to 20μm in this study. Since measurements are taken within the boundary layer, we select a representative height level between 0-100 m.

4.2. Li et al., 1996 – Ground Station – MEE only

Measurements are made over Barbados between 4 April to 3 May 1994 (main measurement period in April). Daily aerosol particles are collected using the Whatman-41 filter, and mineral dust components are determined by ashing the filter at 500 ^{o}C and weighing the residue. The resulting dust size distribution is mostly for particles of diameter $D \leq 10\ \mu m$. Aerosol scattering is measured by nephelometer at 530 nm, and the resulting mass scattering efficiency is determined by linear regression method over the entire period of measurements.

4.3. Li et al., 2000 – Ground Station – MSE only

Measurements were taken at a station on top of the Waliguan Mountain (3816 m atitude), in the Qinghai Province, China during October-November, 1997 and January 1998. Aerosol sizes up to diameter of D ≤ 18 μm were measured by a Micro Orifice Uniform Deposit Impactor used with Teflon filter. Measured $CaCO_3$ are assumed as proxy for dust particles, and consequently for dust volume distribution. Mass scattering efficiency is calculated using the Mie theory with density and index of refraction for $CaCO_3$ taken from Williams (1996). Values are reported at 550 nm wavelength (see their table 2).

4.4. Maring et al., 2000 – Ground Station – MSE only

Dust properties are measured during July 1995 at the Global Atmospheric Watch station, located at Izana, Tenerife, Canary Island. Measurements took place at the station 2360 m above sea level, which is above the inversion level that is typically around 1200 m in summer. The dust size distribution is measured using a scanning mobility particle sizer and aerodynamic particle sizer, with diameter mostly up to about 10 μm (see their Fig. 7; it could also sample to 15 μm with stronger wind speed). Aerosol extinction was measured using nephelometer. The mass scattering efficiency is calculated using two methods, as the average for dusty and non-dusty periods: First, by calculating the linear regression between aerosol mass and its scattering (0.52 $m^2\ g^{-1}$), and secondly by using Mie theory (0.48 $m^2\ g^{-1}$). The values are reported for wavelength of 532 nm.

4.5. Andreae et al., 2002 – ARACHNE – MSE only

Over a remote site in the Negev desert (Sde Boker, Israel), measurements of aerosol properties

were conducted for a period of 2 years (Dec, 1995 –Oct, 1997) as part of Aerosol Radiation and Chemistry Experiment (ARACHNE) research program. For the entire period, light scattering was measured by nephelometer, but every week a 2-days and a 3-days samples are taken using a "Gent" PM10 stacked filter unit sampler to determine the concentration of the constituent species. The mass scattering efficiency is calculated as a multivariate linear regression of the light scattering coefficients on the coarse-mode, fine-mode, sulphate and dust concentrations. Dust mass scattering efficiency at 550 nm is thereafter obtained. For the value correction for non-Lambertian behavior and truncation errors of the nephelometer has been applied.

4.6. Quinn et al., 2002 – INDOEX – MEE only

As part of Indian Ocean Experiment (INDOEX) Intensive Field Phase (IFP), measurements of aerosol properties were made over the Arabia sea and the Indian Ocean on board the R/V Ronald H. Brown between February and March, 1999. The two-stage multi-jet cascade impactors (Berner et al., 1979) apportioned to differential mobility particle sizer and aerodynamic particle sizer are used for size distributions. From the elemental components (Al, Si, Ca, Fe, and Ti), dust is considered as inorganic oxidized material (IOM), and it is obtained by summing the oxides of the elements, in which each elemental mass concentration is multiplied by a molar correction factor (See their Equation 2). The mass extinction efficiency is calculated using Mie theory, and we use here values for particles with diameter $1.1 \leq D \leq 10$ μm, to avoid possible contamination by other aerosol in the sub-micron range (See their Fig. 10). Campaign-derived index of refraction is used. The values are reported for wavelength of 550 nm.

4.7. Haywood et al., 2003 – SHADE – MEE only

Dust particle measurements were taken during the Saharan Dust Experiment (SHADE) which took place between 19-28 September 2000 close to Sal, Cape Verde, off the coast of North Africa. The size distribution is determined using Passive Cavity Aerosol Spectrometer Probe 100X. The size distributions were not corrected for refractive index because they assumed that the refractive index of latex is approximately similar to that of dust. Due to instrument malfunction during the campaign, calculations of optical properties were largely limited to about 10μm. Mie theory is used to calculate the mass extinction efficiency at wavelength of 550 nm (see their table 2).

4.8. Clarke et al. 2004 – ACE-Asia/TRACE-P – PSD and MSE

Aerosol measurements were taken in the Sea of Japan (between Koran and Japan) in the spring (24 February to 10 April) of 2001, as part of the Asian Pacific Regional Aerosol Characterization Experiment (ACE-Asia) and NASA Transport and Chemical Evolution over the Pacific (TRACE-P). Similar instrumentations as the INDOEX campaign (Quinn et al., 2002) were used during ACE-Asia campaign. ACE-Asia used a laser optical particle counters (OPC) and condensation nuclei (CN) counters for aerosol size distribution. The OPC was operated at150°C and then at 300°C, to drive off low-temperature volatiles. In addition, light scattering of coarse and fine aerosol mode was measured by two-wavelength TSI 563 nephelometers. Despite some differences in instrumentations in the ACE-Asia and TRACE-P, the authors show that measured aerosol sizing and optical properties agreed within instrument uncertainty at all altitudes. After the size distribution are normalized to emphasize the coarse dust (see their Fig. 5), we select the resulting reference size distribution as the representative size distribution. In addition, based on their Fig. 1, we choose the representative height level between surface and 6km. The mass scattering efficiency is calculated using the Mie theory. The wavelength is at 550 nm.

4.9. Otto et al., 2007 – ACE-2 – PSD only

Aerosol measurements were taken during Aerosol Characterisation Experiment (ACE-2) conducted about 50—200km off the coast of Northern Africa close to Canary Islands on 8th of July, 1997. The aerosol size distributions used data from five instruments, including Condensation Particle Counter (CPC), Differential Mobility Analyser (DMA), Optical Particle Counter (OPC), and Forward Scattering Spectrometer Probe (FSSP). Together, the instruments measured particles up to diameter of ~31μm (see their Table 1). We use reported size distribution, up to 20μm at four specific levels – 2700 m, 4000 m, 5500 m, 7000 m.

4.10. Chou et al., 2008 & Osborne et al. 2008 – AMMA/DABEX – PSD and MEE

Based in Niamey, Niger, aerosol measurements were made between 13 January and 3 February, 2006 over the West Africa Sahel region, as part of the Dust and Biomass-burning Experiment (DABEX), affiliated with the African Monsoon Multidisciplinary Analysis (AMMA). On board the UK BAe-146 research aircraft , aerosol size distribution are measured using the Passive Cavity Aerosol Spectrometer Probe 100-X (PCASP) with additional counter-flow virtual impactor (CVI) inlet to measure particles up to diameter of 10 μm. Because of the aerosol inlet configuration on the aircraft, the measurement of coarse dust were particularly problematic. Both groups of authors reported size distributions measured from 2 flights numbered B160 and B165 out of 14 flights. Dust size distribution is taken from Chou et al, 2008, while the mass extinction efficiency is taken from Osborne et al., 2008. Since most of the flight are below ~1500m above ground level, we select 0-1500m as the representative height level. The mass extinction efficiency is calculated using Mie theory, at 550 nm wavelength. The mass extinction efficiency is calculated with log-normal fit to the measured dust size distribution, with assumed dust density of 2.65 g cm^{-3} (see Table 4 in Osborne et al, 2008).

4.11. McConnell et al., 2008 – DODO-1/ DODO-2 – PSD and MEE

Based at Dakar, Senegal, measurements of dust properties are conducted as part of the Dust Outflow and Deposition to the Ocean project (DODO) off the coast of North Africa. The project occurred on two phases: One between 7 to 16 February 2006, called DODO-1, and the other between 22 to 28 August, 2006, called DODO-2. During DODO, a combination of wing-mounted Passive Cavity Aerosol Spectrometer Probe (PCASP), Droplet Measurement Technology cloud droplet probe (CDP-100), and bulk filters are used to measure dust size distribution up to diameter of 40 μm. We use the DODO-2 size distribution in this study based on their Fig. 7. Because the height level is given around 1 km altitude for the size distribution (see caption of Fig. 7), we limit our representative height level between 0-1 km. The mass extinction efficiency is calculated with Mie code, using the measured size distribution. Because coarse dust particles are not collected during DODO-1, we use the MEE value reported in Osborne et al., 2008 (see their Table 4) that include coarse dust collected during DABEX.

4.12. Weinzierl et al., 2009 – SAMUM-1 – PSD only

Based in Casablanca, Morocco, in situ dust particle size distribution measurements were taken onboard the German Center for Aviation and Space Flight (DLR) Falcon as part of the Saharan Mineral Dust Experiment (SAMUM-1) in Southern Morocco in May and June 2006. Three dust events were observed during the campaign on 16 to 22 May, 24 to 28 May, and 31 May to 5 June. We use the size distribution measured from a wing-mounted Forward Scattering Spectrometer Probe (FSSP) 300, and the composite size distribution from three Condensation Particle Counters (CPCs) heated with a thermal denuder (TD) at 250°C and a Grimm OPC (Optical Particle Counter). The FSSP-300 measured particles with diameters between 0.3 and 30 μm. The three CPCs measured non-volatile particles in nucleation, Aitken, and accumulation mode, respectively. With the Grimm OPC, non-volatile size distribution was derived for particles smaller than 2.5 μm. Data are taken from their Fig. 8 which represents the composite size distribution for L02 on flight #060519a and L07 on flight #060604a. For these flights, are respectively 4853m

and 3703m above sea level, and therefore approximated to 3700-4900m in our study.

4.13. Wagner et al., 2009 – DARPO – PSD only

Based in Casablanca, Morocco, in situ measurements were performed in May 2006 over Portugal as part of the Desert Aerosols over Portugal (DAPRO) project affiliated with SAMUM (see section 4.12), using essentially the same instrumentation and derivation as Weinzierl et al. (2009) with an additional high spectral resolution lidar. Measurements were conducted at 2300m and 3245m during a flight onboard Falcon aircraft over Évora on 27 May 2006, and size distribution data between 0.01 and 35 μm were presented (see their Fig. 9). Size distribution at the two different heights were very similar. In this study, we take the representative height range between 2300-5000m.

4.14. Kandler et al., 2009 – SAMUM-1 – PSD only

During the 2006 SAMUM campaign, Kandler et al. conducted size distribution measurements by collecting dust samples at a ground station in Tinfou, Morocco where dust events occur often

during summer. However, anthropogenic emissions still exerted a significant impact on particles smaller than 500 nm, despite the remote location of the ground station. Mineral dust dominated particles beyond 500 nm. Employing a combination Differential Mobility Particle Sizer (DMPS), Aerodynamic Particle Sizer (APS) and single-stage impactor (SSI), the authors measured and reported a size distribution under a higher concentration condition, named dust wind condition. The number distribution of particles larger than 500 nm varied by more than one order of magnitude, largely correlated to meteorological conditions. For particles larger than 10 μm, the variation was about three orders of magnitude. Since the station is at an elevation of approximately 684 m above sea level and the inlet of the sampling device ~4 m above ground level, we choose our representative height to be between 0-700m.

4.15. Kandler et al., 2011 – SAMUM-2 – PSD only

A part of the SAMUM-2 campaign which aims to study more aged dust as opposed to fresh dust in SAMUM-1, the effort of Kandler et al. (2011) used the similar instrumentation as SAMUM-1 (Kandler et al., 2009) to measure dust size distribution at a ground station on Praia, Cape Verde in winter 2008. A notably higher concentration of clay minerals was found compared to SAMUM-1, as expected for aged dust. Size distributions from three dust phases were reported. As in SAMUM-1, it was found that wind speed had a significant impact on the distribution between 400 nm and 10 μm, and this strength of this impact increases rapidly beyond 10 μm. The presence of larger particles is highly correlated with mass concentration. Similar to Kandler et al., 2009, because the elevation of the station is approximately 100 m above sea level, we place our representative height levels between 0-110m.

4.16. Ryder et al., 2013a and Ryder et al., 2013b – Fennec 2011 – PSD and MEE

Both Ryder et al studies measured dust properties over and near western side of the North African desert on board the UK's BAe-146-301 Research Aircraft during the Fennec June 2011 campaign. While the Ryder et al., (2013a) study reported dust properties near the Canary Islands, the Ryder et al., (2013b) study reported dust properties farther inland over Mauritania and Mali. Below, we

give brief description of the instruments used and measurements taken. For more details, please refer to their studies.

(Ryder et al., 2013b): Although 16 dedicated flights was conducted over Mauritania and Mali during the campaign, only 11 of those with consistent instrumentation were used. A suite of instruments is used to measure dust size distribution (see table 3 in Ryder et al., 2013b), namely wing-mounted Passive Cavity Aerosol Spectrometer Probe 100X (PCASP), Cloud Droplet Probe (CDP), and Cloud Imaging Probe (CIP). The measurement covers significant coarse-mode size range of dust particles, and were corrected for a refractive index appropriate for dust and for instrumental drift during the campaign. Details of the calibration and correction performed on each instrument can be found in (Ryder et al., 2013b). Since most of the measurements taken are below 2-3 km (see their Fig. 2), therefore in this study we use a representative height between 0-3 km. We use data taken from their Fig. 5b, which include the mean size distribution obtained using the PCASP, CDP and CIP.

(Ryder et al., 2013a): Although dust properties are taken near the Canary Islands, in-situ measurements reported in this study uses similar instrumentations as in (Ryder et al., 2013b). Because take-off and landing profiles observations, vertical distribution of the dust size distribution can be made. We obtain these dataset directly from the authors, and present size distribution at four levels – 2500, 4000, 5500, and 6000 m. As reported in the study, we used here the averaged MEE value of 0.31+/-0.08 between the calculate values for aged dust (0.23) and the SAL categories (0.39). Mie scattering code is used to calculate the mass scattering efficiency at wavelength of 550 nm.

4.17. Jung et al., 2013 – BACEX - PSD only

In situ measurements of aged dust size distribution was conducted onboard Center for Interdisciplinary Remotely Piloted Aircraft Studies (CIRPAS) Twin Otter research aircraft under the Barbados Aerosol Cloud Experiment (BACEX) in on 1 and 2 April 2010. Size distribution measured from Passive Cavity Aerosol Spectrometer Probe (PCASP) and the forward scattering section of a Cloud and Aerosol Spectrometer (CASF) covered particle diameters from 0.1 to 54

μm. Data taken while the aircraft was in clouds were excluded because PCASP is known to have low accuracy inside clouds. We use one measurement on 1 April within the Sahara air layer (SAL) at 2726m, and one on 2 April in the intermediate layer at 1289m. For comparison, the representative height is placed between 1250-2700m. The Mass extinction efficiency is calculated using Mie theory, at 550 nm wavelength.

4.18. Weinzierl et al., 2017 – SALTRACE - PSD only

Based in Barbados, Puerto Rico, and Cabo Verde, in situ aerosol size distribution measurements were conducted as part of the Saharan Aerosol Long-Range Transport and Aerosol–Cloud-Interaction Experiment (SALTRACE) in June 2013. The same air mass was first sampled over Cabo Verde at the altitude of 2.6km on 17 June 2013, and again over Barbados at 2.3km on 22 June 2013. Total number distribution below 1 μm was inverted from measurements from three Condensation Particle Counters (CPCs) between 0.005 and 2.5 μm, a Grimm Sky Optical Particle Counter (OPC) between 0.25 and 2.5 μm, and a wing-mounted Ultra-High Sensitivity Aerosol Spectrometer Airborne (UHSAS-A) between 0.06 and 1 μm. Total number distribution above 1 μm was measured with Cloud and Aerosol Spectrometer with Depolarization (CAS-DPOL). Distribution in the full size range was parametrized with four lognormal distributions. The authors expected 20-μm particles to be removed after 3 days of transport, but 20% of the observed 20-μm particles in Cabo Verde survived in the second measurement above Barbados.

4.19. Ryder et al., 2018 - AER-D - PSD and MEE

In-situ measurements were taken in August, 2015 close to Cape Verde, off the coast of Northern Africa properties during the beginning of trans-Atlantic transport of dust particles. These measurements were part of the AERosol Properties – Dust (AER-D) fieldwork campaign, which ran alongside the Ice in Clouds Experiment – Dust (ICE-D) project, and similarly used the UK's BAe-146-301 Research Aircraft. In addition to the instruments used during Fennec 2011 campaign, the AER-D campaign used cloud imaging probes (CIP15 and 2DS) for size distributions at d>10 microns. They use wing-mounted optical particle counters and shadow probes to measure dust sizes between 0.1 and 100 μm diameter, a nephelometer and an absorption photometer to

measure dust optical properties, and an in-cabin filter collection system to collect dust samples. Data for size distribution was obtained directly from the authors. However, reported value of dust mass extinction efficiency, calculated using Mie code at 550 nm wavelength, was obtained from their paper.

References

Andreae, T. W., Andreae, M. O., Ichoku, C., Maenhaut, W., Cafmeyer, J., Karnieli, A. and Orlovsky, L.: Light scattering by dust and anthropogenic aerosol at a remote site in the Negev desert, Israel, J. Geophys. Res., 107(D2), 4008, doi:10.1029/2001JD900252, 2002.

Barnard, J. C., Fast, J. D., Paredes-Miranda, G., Arnott, W. P. and Laskin, A.: Technical Note: Evaluation of the WRF-Chem "Aerosol Chemical to Aerosol Optical Properties" Module using data from the MILAGRO campaign, Atmos. Chem. Phys., 10(15), 7325–7340, doi:10.5194/acp-10-7325-2010, 2010.

Binkowski, F. S. and Shankar, U.: The Regional Particulate Matter Model: 1. Model description and preliminary results, J. Geophys. Res., 100(D12), 26191, doi:10.1029/95JD02093, 1995.

Buchard, V., Randles, C. A., da Silva, A. M., Darmenov, A., Colarco, P. R., Govindaraju, R., Ferrare, R., Hair, J., Beyersdorf, A. J., Ziemba, L. D., Yu, H., Buchard, V., Randles, C. A., Silva, A. M. da, Darmenov, A., Colarco, P. R., Govindaraju, R., Ferrare, R., Hair, J., Beyersdorf, A. J., Ziemba, L. D. and Yu, H.: The MERRA-2 Aerosol Reanalysis, 1980 Onward. Part II: Evaluation and Case Studies, J. Clim., 30(17), 6851–6872, doi:10.1175/JCLI-D-16-0613.1, 2017.

Chapman, E. G., Gustafson, W. I., Easter, R. C., Barnard, J. C., Ghan, S. J., Pekour, M. S. and Fast, J. D.: Coupling aerosol-cloud-radiative processes in the WRF-Chem model: Investigating the radiative impact of elevated point sources, Atmos. Chem. Phys., 9(3), 945–964, doi:10.5194/acp-9-945-2009, 2009.

Chou, C., Formenti, P., Maille, M., Ausset, P., Helas, G., Harrison, M. and Osborne, S.: Size distribution, shape, and composition of mineral dust aerosols collected during the African Monsoon Multidisciplinary Analysis Special Observation Period 0: Dust and Biomass-Burning Experiment field campaign in Niger, January 2006, J. Geophys. Res., 113(D23), D00C10, doi:10.1029/2008JD009897, 2008.

Clarke, A. D., Shinozuka, Y., Kapustin, V. N., Howell, S., Huebert, B., Doherty, S., Anderson,

T., Covert, D., Anderson, J., Hua, X., Moore, K. G., McNaughton, C., Carmichael, G. and Weber, R.: Size distributions and mixtures of dust and black carbon aerosol in Asian outflow: Physiochemistry and optical properties, J. Geophys. Res., 109(D15), D15S09, doi:10.1029/2003JD004378, 2004.

Colarco, P., Silva, A., Chin, M. and Diehl, T.: Online simulations of global aerosol distributions in the NASA GEOS - 4 model and comparisons to satellite and ground - based aerosol optical depth, , 115, doi:10.1029/2009JD012820, 2010.

D'Almeida, G. A.: On the variability of desert aerosol radiative characteristics, J. Geophys. Res., 92(D3), 3017, doi:10.1029/JD092iD03p03017, 1987.

D'Almeida, G. A. and Schutz, L.: Number, mass and volume distributions of mineral aerosol and soils of the Sahara., J. Clim. Appl. Meteorol., 22(2), 233–243, doi:10.1175/1520-0450(1983)022<0233:NMAVDO>2.0.CO;2, 1983.

Easter, R. C., Ghan, S. J., Zhang, Y., Saylor, R. D., Chapman, E. G., Laulainen, N. S., Abdul-Razzak, H., Leung, L. R., Bian, X. and Zaveri, R. A.: MIRAGE: Model description and evaluation of aerosols and trace gases, J. Geophys. Res., 109(D20), D20210, doi:10.1029/2004JD004571, 2004.

Fast, J. D., Gustafson, W. I., Easter, R. C., Zaveri, R. A., Barnard, J. C., Chapman, E. G., Grell, G. A. and Peckham, S. E.: Evolution of ozone, particulates, and aerosol direct radiative forcing in the vicinity of Houston using a fully coupled meteorology-chemistry-aerosol model, J. Geophys. Res., 111(D21), D21305, doi:10.1029/2005JD006721, 2006.

Flemming, J., Huijnen, V., Arteta, J., Bechtold, P., Beljaars, A., Blechschmidt, A.-M., Diamantakis, M., Engelen, R. J., Gaudel, A., Inness, A., Jones, L., Josse, B., Katragkou, E., Marecal, V., Peuch, V.-H., Richter, A., Schultz, M. G., Stein, O. and Tsikerdekis, A.: Tropospheric chemistry in the Integrated Forecasting System of ECMWF, Geosci. Model Dev., 8(4), 975–1003, doi:10.5194/gmd-8-975-2015, 2015.

Flemming, J., Benedetti, A., Inness, A., Engelen, R. J., Jones, L., Huijnen, V., Remy, S., Parrington, M., Suttie, M., Bozzo, A., Peuch, V.-H., Akritidis, D. and Katragkou, E.: The CAMS interim Reanalysis of Carbon Monoxide, Ozone and Aerosol for 2003–2015, Atmos. Chem. Phys., 17(3), 1945–1983, doi:10.5194/acp-17-1945-2017, 2017.

Gelaro, R., McCarty, W., Suárez, M. J., Todling, R., Molod, A., Takacs, L., Randles, C. A., Darmenov, A., Bosilovich, M. G., Reichle, R., Wargan, K., Coy, L., Cullather, R., Draper, C.,

Akella, S., Buchard, V., Conaty, A., da Silva, A. M., Gu, W., Kim, G.-K., Koster, R., Lucchesi, R., Merkova, D., Nielsen, J. E., Partyka, G., Pawson, S., Putman, W., Rienecker, M., Schubert, S. D., Sienkiewicz, M., Zhao, B., Gelaro, R., McCarty, W., Suárez, M. J., Todling, R., Molod, A., Takacs, L., Randles, C. A., Darmenov, A., Bosilovich, M. G., Reichle, R., Wargan, K., Coy, L., Cullather, R., Draper, C., Akella, S., Buchard, V., Conaty, A., Silva, A. M. da, Gu, W., Kim, G.-K., Koster, R., Lucchesi, R., Merkova, D., Nielsen, J. E., Partyka, G., Pawson, S., Putman, W., Rienecker, M., Schubert, S. D., Sienkiewicz, M. and Zhao, B.: The Modern-Era Retrospective Analysis for Research and Applications, Version 2 (MERRA-2), J. Clim., 30(14), 5419–5454, doi:10.1175/JCLI-D-16-0758.1, 2017.

Gerber, H.: Supersaturation and Droplet Spectral Evolution in Fog, J. Atmos. Sci., 48(24), 2569–2588, doi:10.1175/1520-0469(1991)048<2569:SADSEI>2.0.CO;2, 1991.

Ginoux, P., Chin, M., Tegen, I., Prospero, J. M., Holben, B., Dubovik, O. and Lin, S.-J.: Sources and distributions of dust aerosols simulated with the GOCART model, J. Geophys. Res. Atmos., 106(D17), 20255–20273, doi:10.1029/2000JD000053, 2001.

Giorgi, F. and Chameides, W. L.: Rainout lifetimes of highly soluble aerosols and gases as inferred from simulations with a general circulation model, J. Geophys. Res., 91(D13), 14367, doi:10.1029/JD091iD13p14367, 1986.

Grell, G. A., Peckham, S. E., Schmitz, R., McKeen, S. A., Frost, G., Skamarock, W. C. and Eder, B.: Fully coupled “online” chemistry within the WRF model, Atmos. Environ., 39(37), 6957–6975, doi:10.1016/J.ATMOSENV.2005.04.027, 2005.

Haywood, J.: Radiative properties and direct radiative effect of Saharan dust measured by the C-130 aircraft during SHADE: 1. Solar spectrum, J. Geophys. Res., 108(D18), 8577, doi:10.1029/2002JD002687, 2003.

Hess, M., Koepke, P., Schult, I., Hess, M., Koepke, P. and Schult, I.: Optical Properties of Aerosols and Clouds: The Software Package OPAC, Bull. Am. Meteorol. Soc., 79(5), 831–844, doi:10.1175/1520-0477(1998)079<0831:OPOAAC>2.0.CO;2, 1998.

Hogan, T. F. and Brody, L. R.: Sensitivity Studies of the Navy’s Global Forecast Model Parameterizations and Evaluation of Improvements to NOGAPS, Mon. Weather Rev., 121(8), 2373–2395, doi:10.1175/1520-0493(1993)121<2373:SSOTNG>2.0.CO;2, 1993.

Hogan, T. F. and Rosmond, T. E.: The Description of the Navy Operational Global Atmospheric Prediction System’s Spectral Forecast Model, Mon. Weather Rev., 119(8), 1786–1815,

doi:10.1175/1520-0493(1991)119<1786:TDOTNO>2.0.CO;2, 1991.
Hyer, E. J., Reid, J. S. and Zhang, J.: An over-land aerosol optical depth data set for data assimilation by filtering, correction, and aggregation of MODIS Collection 5 optical depth retrievals, Atmos. Meas. Tech., 4(3), 379–408, doi:10.5194/amt-4-379-2011, 2011.
Inness, A., Blechschmidt, A.-M., Bouarar, I., Chabrillat, S., Crepulja, M., Engelen, R. J., Eskes, H., Flemming, J., Gaudel, A., Hendrick, F., Huijnen, V., Jones, L., Kapsomenakis, J., Katragkou, E., Keppens, A., Langerock, B., de Mazière, M., Melas, D., Parrington, M., Peuch, V. H., Razinger, M., Richter, A., Schultz, M. G., Suttie, M., Thouret, V., Vrekoussis, M., Wagner, A. and Zerefos, C.: Data assimilation of satellite-retrieved ozone, carbon monoxide and nitrogen dioxide with ECMWF's Composition-IFS, Atmos. Chem. Phys., 15(9), 5275–5303, doi:10.5194/acp-15-5275-2015, 2015.
Ito, A. and Kok, J. F.: Do dust emissions from sparsely vegetated regions dominate atmospheric iron supply to the Southern Ocean?, J. Geophys. Res. Atmos., 122(7), 3987–4002, doi:10.1002/2016JD025939, 2017.
Ito, A., Sillman, S. and Penner, J. E.: Effects of additional nonmethane volatile organic compounds, organic nitrates, and direct emissions of oxygenated organic species on global tropospheric chemistry, J. Geophys. Res., 112(D6), D06309, doi:10.1029/2005JD006556, 2007.
Jacob, D., Liu, H. and Yantosca, R.: Harvard wet deposition scheme for GMI, Harvard Univ. Atmos. Chem. Model. Gr., n/a(n/a), n/a, 2000.
Joyce, R. J., Janowiak, J. E., Arkin, P. A., Xie, P., Joyce, R. J., Janowiak, J. E., Arkin, P. A. and Xie, P.: CMORPH: A Method that Produces Global Precipitation Estimates from Passive Microwave and Infrared Data at High Spatial and Temporal Resolution, J. Hydrometeorol., 5(3), 487–503, doi:10.1175/1525-7541(2004)005<0487:CAMTPG>2.0.CO;2, 2004.
Jung, E., Albrecht, B., Prospero, J. M., Jonsson, H. H. and Kreidenweis, S. M.: Vertical structure of aerosols, temperature, and moisture associated with an intense African dust event observed over the eastern Caribbean, J. Geophys. Res. Atmos., 118(10), 4623–4643, doi:10.1002/jgrd.50352, 2013.
Kandler, K., SchüTZ, L., Deutscher, C., Ebert, M., Hofmann, H., JäCKEL, S., Jaenicke, R., Knippertz, P., Lieke, K., Massling, A., Petzold, A., Schladitz, A., Weinzierl, B., Wiedensohler, A., Zorn, S. and Weinbruch1, S.: Size distribution, mass concentration, chemical and mineralogical composition and derived optical parameters of the boundary layer aerosol at

Tinfou, Morocco, during SAMUM 2006, Tellus B Chem. Phys. Meteorol., 61(1), 32–50, doi:10.1111/j.1600-0889.2008.00385.x, 2009.
Kandler, K., Lieke, K., Benker, N., Emmel, C., Küpper, M., Müller-Ebert, D., Ebert, M., Scheuvens, D., Schladitz, A., Schütz, L. and Weinbruch, S.: Electron microscopy of particles collected at Praia, Cape Verde, during the Saharan Mineral Dust Experiment: particle chemistry, shape, mixing state and complex refractive index, Tellus B Chem. Phys. Meteorol., 63(4), 475–496, doi:10.1111/j.1600-0889.2011.00550.x, 2011.
Kok, J. F.: A scaling theory for the size distribution of emitted dust aerosols suggests climate models underestimate the size of the global dust cycle, Proc. Natl. Acad. Sci., 108(3), 1016–1021, doi:10.1073/pnas.1014798108, 2011.
Kok, J. F., Albani, S., Mahowald, N. M. and Ward, D. S.: An improved dust emission model - Part 2: Evaluation in the Community Earth System Model, with implications for the use of dust source functions, Atmos. Chem. Phys., 14(23), 13043–13061, doi:10.5194/acp-14-13043-2014, 2014a.
Kok, J. F., Mahowald, N. M., Fratini, G., Gillies, J. A., Ishizuka, M., Leys, J. F., Mikami, M., Park, M.-S., Park, S.-U., Van Pelt, R. S. and Zobeck, T. M.: An improved dust emission model – Part 1: Model description and comparison against measurements, Atmos. Chem. Phys., 14(23), 13023–13041, doi:10.5194/acp-14-13023-2014-supplement, 2014b.
Li, S.-M., Tang, J., Xue, H. and Toom-Sauntry, D.: Size distribution and estimated optical properties of carbonate, water soluble organic carbon, and sulfate in aerosols at a remote high altitude site in western China, Geophys. Res. Lett., 27(8), 1107–1110, doi:10.1029/1999GL010929, 2000.
Li, X., Maring, H., Savoie, D., Voss, K. and Prospero, J. M.: Dominance of mineral dust in aerosol light-scattering in the North Atlantic trade winds, Nature, 380(6573), 416–419, doi:10.1038/380416a0, 1996.
Liu, H., Jacob, D. J., Bey, I. and Yantosca, R. M.: Constraints from ^{210}Pb and ^{7}Be on wet deposition and transport in a global three-dimensional chemical tracer model driven by assimilated meteorological fields, J. Geophys. Res. Atmos., 106(D11), 12109–12128, doi:10.1029/2000JD900839, 2001.
Liu, X., Penner, J. E. and Herzog, M.: Global modeling of aerosol dynamics: Model description, evaluation, and interactions between sulfate and nonsulfate aerosols, J. Geophys. Res., 110(D18),

D18206, doi:10.1029/2004JD005674, 2005.
Lynch, P., Reid, J. S., Westphal, D. L., Zhang, J., Hogan, T. F., Hyer, E. J., Curtis, C. A., Hegg, D. A., Shi, Y., Campbell, J. R., Rubin, J. I., Sessions, W. R., Turk, F. J. and Walker, A. L.: An 11-year global gridded aerosol optical thickness reanalysis (v1.0) for atmospheric and climate sciences, Geosci. Model Dev., 9(4), 1489–1522, doi:10.5194/gmd-9-1489-2016, 2016.
Maring, H., Savoie, D. L., Izaguirre, M. A., McCormick, C., Arimoto, R., Prospero, J. M. and Pilinis, C.: Aerosol physical and optical properties and their relationship to aerosol composition in the free troposphere at Izaña, Tenerife, Canary Islands, during July 1995, J. Geophys. Res. Atmos., 105(D11), 14677–14700, doi:10.1029/2000JD900106, 2000.
Marticorena, B. and Bergametti, G.: Modeling the atmospheric dust cycle: 1. Design of a soil-derived dust emission scheme, J. Geophys. Res., 100(D8), 16415, doi:10.1029/95JD00690, 1995.
Masson, V., Champeaux, J.-L., Chauvin, F., Meriguet, C., Lacaze, R., Masson, V., Champeaux, J.-L., Chauvin, F., Meriguet, C. and Lacaze, R.: A Global Database of Land Surface Parameters at 1-km Resolution in Meteorological and Climate Models, J. Clim., 16(9), 1261–1282, doi:10.1175/1520-0442-16.9.1261, 2003.
Mccarty, W., Coy, L., Gelaro, R., Huang, A., Merkova, D., Smith, E. B., Sienkiewicz, M., Wargan, K. and Koster, R. D.: MERRA-2 Input Observations: Summary and Assessment. Technical Report Series on Global Modeling and Data Assimilation., 2016.
McConnell, C. L., Highwood, E. J., Coe, H., Formenti, P., Anderson, B., Osborne, S., Nava, S., Desboeufs, K., Chen, G. and Harrison, M. A. J.: Seasonal variations of the physical and optical characteristics of Saharan dust: Results from the Dust Outflow and Deposition to the Ocean (DODO) experiment, J. Geophys. Res., 113(D14), D14S05, doi:10.1029/2007JD009606, 2008.
Michou, M., Nabat, P. and Saint-Martin, D.: Development and basic evaluation of a prognostic aerosol scheme (v1) in the CNRM Climate Model CNRM-CM6, Geosci. Model Dev., 8(3), 501–531, doi:10.5194/gmd-8-501-2015, 2015.
Morcrette, J.-J., Boucher, O., Jones, L., Salmond, D., Bechtold, P., Beljaars, A., Benedetti, A., Bonet, A., Kaiser, J. W., Razinger, M., Schulz, M., Serrar, S., Simmons, A. J., Sofiev, M., Suttie, M., Tompkins, A. M. and Untch, A.: Aerosol analysis and forecast in the European Centre for Medium-Range Weather Forecasts Integrated Forecast System: Forward modeling, J. Geophys. Res., 114(D6), D06206, doi:10.1029/2008JD011235, 2009.
Nabat, P., Somot, S., Mallet, M., Michou, M., Sevault, F., Driouech, F., Meloni, D., di Sarra, A.,

Di Biagio, C., Formenti, P., Sicard, M., Léon, J.-F. and Bouin, M.-N.: Dust aerosol radiative effects during summer 2012 simulated with a coupled regional aerosol–atmosphere–ocean model over the Mediterranean, Atmos. Chem. Phys., 15(6), 3303–3326, doi:10.5194/acp-15-3303-2015, 2015.

Osborne, S. R., Johnson, B. T., Haywood, J. M., Baran, A. J., Harrison, M. A. J. and McConnell, C. L.: Physical and optical properties of mineral dust aerosol during the Dust and Biomass-burning Experiment, J. Geophys. Res., 113(D23), D00C03, doi:10.1029/2007JD009551, 2008.

Otto, S., de Reus, M., Trautmann, T., Thomas, A., Wendisch, M. and Borrmann, S.: Atmospheric radiative effects of an in situ measured Saharan dust plume and the role of large particles, Atmos. Chem. Phys., 7(18), 4887–4903, doi:10.5194/acp-7-4887-2007, 2007.

Quinn, P. K., D. J. Coffman, T. S. Bates, T. L. Miller, J. E. Johnson, E. J. Welton, C. Neusüss, M. Miller and Sheridan, P. J.: Aerosol optical properties during INDOEX 1999: Means, variability, and controlling factors, J. Geophys. Res., 107(D19), 8020, doi:10.1029/2000JD000037, 2002.

Randles, C. A., da Silva, A. M., Buchard, V., Colarco, P. R., Darmenov, A., Govindaraju, R., Smirnov, A., Holben, B., Ferrare, R., Hair, J., Shinozuka, Y., Flynn, C. J., Randles, C. A., Silva, A. M. da, Buchard, V., Colarco, P. R., Darmenov, A., Govindaraju, R., Smirnov, A., Holben, B., Ferrare, R., Hair, J., Shinozuka, Y. and Flynn, C. J.: The MERRA-2 Aerosol Reanalysis, 1980 Onward. Part I: System Description and Data Assimilation Evaluation, J. Clim., 30(17), 6823–6850, doi:10.1175/JCLI-D-16-0609.1, 2017.

Reddy, M. S., Boucher, O., Bellouin, N., Schulz, M., Balkanski, Y., Dufresne, J. and Pham, M.: Estimates of global multicomponent aerosol optical depth and direct radiative perturbation in the Laboratoire de Météorologie Dynamique general circulation model, J. Geophys. Res., 110(D10), D10S16, doi:10.1029/2004JD004757, 2005.

Reichle, R. H., Liu, Q. and Koster, R. D.: Observation-Corrected Precipitation Estimates in GEOS-5. Technical Report Series on Global Modeling and Data Assimilation., 2014.

Reichle, R. H., Liu, Q., Koster, R. D., Draper, C. S., Mahanama, S. P. P., Partyka, G. S., Reichle, R. H., Liu, Q., Koster, R. D., Draper, C. S., Mahanama, S. P. P. and Partyka, G. S.: Land Surface Precipitation in MERRA-2, J. Clim., 30(5), 1643–1664, doi:10.1175/JCLI-D-16-0570.1, 2017.

Rotman, D. A., Atherton, C. S., Bergmann, D. J., Cameron-Smith, P. J., Chuang, C. C., Connell, P. S., Dignon, J. E., Franz, A., Grant, K. E., Kinnison, D. E., Molenkamp, C. R., Proctor, D. D.

and Tannahill, J. R.: IMPACT, the LLNL 3-D global atmospheric chemical transport model for the combined troposphere and stratosphere: Model description and analysis of ozone and other trace gases, J. Geophys. Res. Atmos., 109(D4), n/a-n/a, doi:10.1029/2002JD003155, 2004.
Ryder, C. L., Highwood, E. J., Lai, T. M., Sodemann, H. and Marsham, J. H.: Impact of atmospheric transport on the evolution of microphysical and optical properties of Saharan dust, Geophys. Res. Lett., 40(10), 2433–2438, doi:10.1002/grl.50482, 2013a.
Ryder, C. L., Highwood, E. J., Rosenberg, P. D., Trembath, J., Brooke, J. K., Bart, M., Dean, A., Crosier, J., Dorsey, J., Brindley, H., Banks, J., Marsham, J. H., McQuaid, J. B., Sodemann, H. and Washington, R.: Optical properties of Saharan dust aerosol and contribution from the coarse mode as measured during the Fennec 2011 aircraft campaign, Atmos. Chem. Phys., 13(1), 303–325, doi:10.5194/acp-13-303-2013, 2013b.
Ryder, C. L., Marenco, F., Brooke, J. K., Estelles, V., Cotton, R., Formenti, P., McQuaid, J. B., Price, H. C., Liu, D., Ausset, P., Rosenberg, P., Taylor, J. W., Choularton, T., Bower, K., Coe, H., Gallagher, M., Crosier, J., Lloyd, G., Highwood, E. J. and Murray, B. J.: Coarse mode mineral dust size distributions, composition and optical properties from AER-D aircraft measurements over the Tropical Eastern Atlantic, Atmos. Chem. Phys. Discuss., 1–49, doi:10.5194/acp-2018-739, 2018.
Seinfeld, J. and Pandis, S.: Atmospheric Chemistry and Physics: From Air Pollution to Climate Change., 2006.
Shao, Y., Raupach, M. and Leys, J.: A model for predicting aeolian sand drift and dust entrainment on scales from paddock to region, Aust. J. Soil Res., 34(3), 309, doi:10.1071/SR9960309, 1996.
Shi, Y., Zhang, J., Reid, J. S., Holben, B., Hyer, E. J. and Curtis, C.: An analysis of the collection 5 MODIS over-ocean aerosol optical depth product for its implication in aerosol assimilation, Atmos. Chem. Phys., 11(2), 557–565, doi:10.5194/acp-11-557-2011, 2011.
Stauffer, D. R. and Seaman, N. L.: Use of Four-Dimensional Data Assimilation in a Limited-Area Mesoscale Model. Part I: Experiments with Synoptic-Scale Data, Mon. Weather Rev., 118(6), 1250–1277, doi:10.1175/1520-0493(1990)118<1250:UOFDDA>2.0.CO;2, 1990.
Tanaka, T. Y. and Chiba, M.: Global Simulation of Dust Aerosol with a Chemical Transport Model, MASINGAR, J. Meteorol. Soc. Japan. Ser. II, 83A(0), 255–278, doi:10.2151/jmsj.83A.255, 2005.

Tanaka, T. Y., Orito, K., Sekiyama, T. T., Shibata, K., Chiba, M. and Tanaka, H.: MASINGAR, a global tropospheric aerosol chemical transport model coupled with MRI/JMA98 GCM: Model description, Pap. Meteorol. Geophys., 53(4), 119–138, doi:10.2467/mripapers.53.119, 2003.
Wagner, F., Bortoli, D., Pereira, S., Costa, M. Jo., Maria Silva, A., Weinzierl, B., Esselborn, M., Petzold, A., Rasp, K., Heinold, B. and Tegen, I.: Properties of dust aerosol particles transported to Portugal from the Sahara desert, Tellus B Chem. Phys. Meteorol., 61(1), 297–306, doi:10.1111/j.1600-0889.2008.00393.x, 2009.
Weinzierl, B., Petzold, A., Esselborn, M., Wirth, M., Rasp, K., Kandler, K., SchüTZ, L., Koepke, P. and Fiebig, M.: Airborne measurements of dust layer properties, particle size distribution and mixing state of Saharan dust during SAMUM 2006, Tellus B Chem. Phys. Meteorol., 61(1), 96–117, doi:10.1111/j.1600-0889.2008.00392.x, 2009.
Weinzierl, B., Ansmann, A., Prospero, J. M., Althausen, D., Benker, N., Chouza, F., Dollner, M., Farrell, D., Fomba, W. K., Freudenthaler, V., Gasteiger, J., Groß, S., Haarig, M., Heinold, B., Kandler, K., Kristensen, T. B., Mayol-Bracero, O. L., Müller, T., Reitebuch, O., Sauer, D., Schäfler, A., Schepanski, K., Spanu, A., Tegen, I., Toledano, C., Walser, A., Weinzierl, B., Ansmann, A., Prospero, J. M., Althausen, D., Benker, N., Chouza, F., Dollner, M., Farrell, D., Fomba, W. K., Freudenthaler, V., Gasteiger, J., Groß, S., Haarig, M., Heinold, B., Kandler, K., Kristensen, T. B., Mayol-Bracero, O. L., Müller, T., Reitebuch, O., Sauer, D., Schäfler, A., Schepanski, K., Spanu, A., Tegen, I., Toledano, C. and Walser, A.: The Saharan Aerosol Long-Range Transport and Aerosol–Cloud-Interaction Experiment: Overview and Selected Highlights, Bull. Am. Meteorol. Soc., 98(7), 1427–1451, doi:10.1175/BAMS-D-15-00142.1, 2017.
Williams, M. L.: CRC Handbook of Chemistry and Physics, 76th edition, Occup. Environ. Med., 53(7), 504, 1996.
Xu, L. and Penner, J. E.: Global simulations of nitrate and ammonium aerosols and their radiative effects, Atmos. Chem. Phys., 12(20), 9479–9504, doi:10.5194/acp-12-9479-2012, 2012.
Yoshimura, H. and Yukimoto, S.: Development of a Simple Coupler (Scup) for Earth System Modeling, Pap. Meteorol. Geophys., 59, 19–29, doi:10.2467/mripapers.59.19, 2008.
Yukimoto, S., ADACHI, Y., HOSAKA, M., SAKAMI, T., YOSHIMURA, H., HIRABARA, M., TANAKA, T. Y., SHINDO, E., TSUJINO, H., DEUSHI, M., MIZUTA, R., YABU, S., OBATA, A., NAKANO, H., KOSHIRO, T., OSE, T. and KITOH, A.: A New Global Climate Model of

the Meteorological Research Institute: MRI-CGCM3 ^|^mdash;Model Description and Basic Performance^|^mdash;, J. Meteorol. Soc. Japan, 90A(0), 23–64, doi:10.2151/jmsj.2012-A02, 2012.
Yumimoto, K., Tanaka, T. Y., Oshima, N. and Maki, T.: JRAero: the Japanese Reanalysis for Aerosol v1.0, Geosci. Model Dev., 10(9), 3225–3253, doi:10.5194/gmd-10-3225-2017, 2017.
Zaveri, R. A. and Peters, L. K.: A new lumped structure photochemical mechanism for large-scale applications, J. Geophys. Res. Atmos., 104(D23), 30387–30415, doi:10.1029/1999JD900876, 1999.
Zaveri, R. A., Easter, R. C., Fast, J. D. and Peters, L. K.: Model for Simulating Aerosol Interactions and Chemistry (MOSAIC), J. Geophys. Res., 113(D13), D13204, doi:10.1029/2007JD008782, 2008.
Zhang, J. and Reid, J. S.: MODIS aerosol product analysis for data assimilation: Assessment of over-ocean level 2 aerosol optical thickness retrievals, J. Geophys. Res., 111(D22), D22207, doi:10.1029/2005JD006898, 2006.
Zhang, J., Reid, J. S., Westphal, D. L., Baker, N. L. and Hyer, E. J.: A system for operational aerosol optical depth data assimilation over global oceans, J. Geophys. Res., 113(D10), D10208, doi:10.1029/2007JD009065, 2008.
Zhang, L., Gong, S., Padro, J. and Barrie, L.: A size-segregated particle dry deposition scheme for an atmospheric aerosol module, Atmos. Environ., 35(3), 549–560, doi:10.1016/S1352-2310(00)00326-5, 2001.
Zhao, C., Wang, Y., Yang, Q., Fu, R., Cunnold, D. and Choi, Y.: Impact of East Asian summer monsoon on the air quality over China: View from space, J. Geophys. Res., 115(D9), D09301, doi:10.1029/2009JD012745, 2010a.
Zhao, C., Liu, X., Leung, L. R., Johnson, B., McFarlane, S. A., Gustafson, W. I., Fast, J. D. and Easter, R.: The spatial distribution of mineral dust and its shortwave radiative forcing over North Africa: modeling sensitivities to dust emissions and aerosol size treatments, Atmos. Chem. Phys., 10(18), 8821–8838, doi:10.5194/acp-10-8821-2010, 2010b.
Zhao, C., Liu, X., Ruby Leung, L. and Hagos, S.: Radiative impact of mineral dust on monsoon precipitation variability over West Africa, Atmos. Chem. Phys., 11(5), 1879–1893, doi:10.5194/acp-11-1879-2011, 2011.
Zhao, C., Chen, S., Leung, L. R., Qian, Y., Kok, J. F., Zaveri, R. A. and Huang, J.: Uncertainty

in modeling dust mass balance and radiative forcing from size parameterization, , 13(21), 10733–10753, doi:10.5194/acp-13-10733-2013, 2013.